Available online at www.sciencedirect.com
ScienceDirect
Trans. Nonferrous Met. Soc. China 25(2015) 3657−3663
Transactions of Nonferrous Metals Society of China
www.tnmsc.cn

Morphology, photoluminescence and gas sensing of Ce-doped ZnO microspheres

Yan LI, Jin-cheng LIU, Xiao-xue LIAN, Tan LÜ, Fang-xian ZHAO

College of Science, Civil Aviation University of China, Tianjin 300300, China

Received 29 December 2014; accepted 17 June 2015

Abstract: Ce-doped ZnO microspheres were solvothermally prepared, and their microstructure, morphology, photoluminescence, and gas sensing were investigated by X-ray diffractometer, field emission scanning electron microscopy, transmission electron microscopy, fluorescence spectrometer and gas sensing analysis system. The results showed that the Ce-doped ZnO microspheres were composed of numerous nanorods with a diameter of 70 nm and a wurtzite structure. Ce-doping could cause a morphological transition from loose nanorods assembly to a tightly assembly in the microspheres. Compared with pure ZnO, the photoluminescence of the Ce-doped microspheres showed red-shifted UV emission and an enhanced blue emission. Particularly, the Ce-doped ZnO sensors exhibited much higher sensitivity and selectivity to ethanol than that of pure ZnO sensor at 320 °C. The ZnO microspheres doped with 6% Ce (mole fraction) exhibited the highest sensitivity (about 30) with rapid response (2 s) and recovery time (16 s) to 50×10^{-6} ethanol gas.

Key words: Ce-doping; ZnO; morphology; microspheres; gas sensing; photoluminescence

1 Introduction

As a nontoxic and inexpensive n-type semiconductor, ZnO offers a promising candidate for various applications, due to its exceptional properties such as wide band gap (3.37 eV) and high exciton binding energy (60 meV) at room temperature. Many efforts have been paid to the synthesis of ZnO nanostructures including nanowires [1], nanotubes [2], nanofilm [3], flower-like structure [4], and hollow spheres [5], which have drawn intensive investigation owing to their potential applications in various functional devices, such as field-effect transistor [6], solar cells [7], light emitting devices [8], and gas sensors [9,10]. Recently, interest in ZnO hierarchical micro/nanospheres has been greatly stimulated for their large specific surface area and porous shell, which offers greater opportunity for diffusion, mass transportation, and surface reactions. Therefore, ZnO with hierarchical nanostructures is thought to be good for the gas-sensing, catalytic, and photovoltaic applications [11]. For instance, SONG et al [12] prepared ZnO hollow spheres to detect acetone. Generally, the template-free solvothermal method is considered a very simple and convenient method for preparing ZnO hierarchical micro/nanospheres in comparison with template method, which accompanies the use of removable or sacrificial templates. Doping ZnO with selective elements, e.g., noble metals [13], transition metal oxides [14], rare-earth metals [15] and main-group metal oxides [16], has been considered as effective methods to modify optical, magnetic, electrical and gas-sensing properties of semiconductor materials. Rare earth-doped ZnO is technologically important, as it has potential applications for making efficient luminescent and gas-sensing materials. In particular, Ce as a dopant could enhance gas-sensing properties by mending the morphology, changing energy band structure and creating more active adsorption sites. In order to mend optical and gas-sensing performance, considerable efforts have been devoted to preparing Ce-doped ZnO. YANG et al [17] reported a sol–gel method with low annealing temperature of 500 °C for preparing Ce-doped nanorod, which shows good optical properties at room temperature. WAN et al [18] fabricated Ce-doped ZnO nanofibers by

Foundation item: Project (61079010) supported by the National Natural Science Foundation of China and the Civil Aviation Administration of China; Project (3122013P001) supported by the Significant Pre-research Funds of Civil Aviation University of China; Project (MHRD20140209) supported by the Science and Technology Innovation Guide Funds of Civil Aviation Administration of China

Corresponding author: Yan LI; Tel/Fax: +86-22-24092514; E-mail: liyan01898@163.com

DOI: 10.1016/S1003-6326(15)64006-7

electrospinning method, and the fibers-based sensor exhibits better sensing properties than pure ZnO nanofibers sensor. Also, SIN et al [19] investigated the enhanced photocatalytic activity of rare earth-doped ZnO hierarchical micro/nanospheres under visible light irradiation. These relevant studies with an objective to determine the influence of controllable doping were mainly focused on the promoting effect of Ce doping. However, up to date, a considerable amount of research has proved that the size and morphology of ZnO nano-materials have great influence on their performances [20]. Therefore, the morphology modification induced by Ce-doping may also play a vital role in their properties, which is necessary for further study.

In this work, the pure and Ce-doped ZnO microspheres were synthesized by a simple solvothermal route without any templates. The effects of Ce doping on the morphological modification, photoluminescence and gas-sensing of ZnO microspheres were investigated. Additionally, the sensing mechanism was also discussed.

2 Experimental

Ce-doped ZnO hierarchical microspheres were prepared as follows. 1.0 g zinc acetate dihydrate was dissolved in 8 mL of deionized water and then mixed with 60 mL glycerol under intense mechanical stirring for 1 h. The resulting mixture was transferred into a Teflon lined autoclave, sealed and maintained at 200 °C for 5 h. Afterwards, the autoclave was cooled to room temperature. Finally, the white precipitate was separated by centrifugation, washed with deionized water and ethanol several times, and dried at 60 °C for 10 h. Ce (2%−10%, mole fraction)-doped ZnO microphones were prepared by taking the same procedure except appropriate amount of cerium acetate was dissolved in zinc acetate dihydrate solution at the beginning of the reaction process. All the reagents used in the experiments were of analytical grade without further purification.

The morphological analysis of ZnO microspheres was performed by field emission scanning electron microscopy (X−650, Hitachi, Japan). X-ray diffraction (XRD) patterns of the products were obtained using a DX–2000 X-ray diffractometer with Cu K_{α} radiation (λ=0.154184 nm), operated at 40 kV and 25 mA in the 2θ range from 20° to 70°. Photoluminescence (PL) emission spectra were conducted on a spectrophotometer (F−7000, Hitachi, Japan) at room temperature using 325 nm as the excitation wavelength. The gas-sensing properties were measured on a CGS–8 intelligent gas sensing analysis system.

The fabrication and testing procedure of gas sensor are similar to that described in Ref. [21]. Firstly, the as-prepared samples were dispersed in deionized water to form a paste, which was then coated onto the surface of an alumina tube. A Ni–Cr wire was inserted into the tube as a heater to control operating temperature and welded on the sensor pedestal. In order to ensure the stability and reliability, the gas sensors were heat-treated at 500 °C for 3 h. The gas-sensing measurement was performed on the CGS−8 intelligent gas sensing analysis system (Beijing Elite Tech Co., Ltd., China). The gas sensitivity (S) was defined as $S=R_a/R_g$, where R_a and R_g are sensor resistances in the air and target gas, respectively.

3 Results and discussion

The XRD patterns of the Ce-doped ZnO microspheres are presented in Fig. 1. All the diffraction peaks in the XRD spectra match well with those given by JCPDS card No. 36−1451, which indicated that all the samples had typical hexagonal wurtzite structures. No diffraction peaks of Ce or other impurity phases were detected, thus we assume that the Ce ions have uniformly substituted into the Zn^{2+} sites or interstitial sites in the ZnO lattice. In comparison, the intensity of the XRD peaks was reduced after introducing Ce into ZnO microspheres. In order to prove the existence of Ce-dopant in ZnO structure, EDS analysis was carried out for all samples, and the results show that all Ce-doped ZnO is composed of Ce, Zn and O elements, except the pure ZnO containing Zn and O elements.

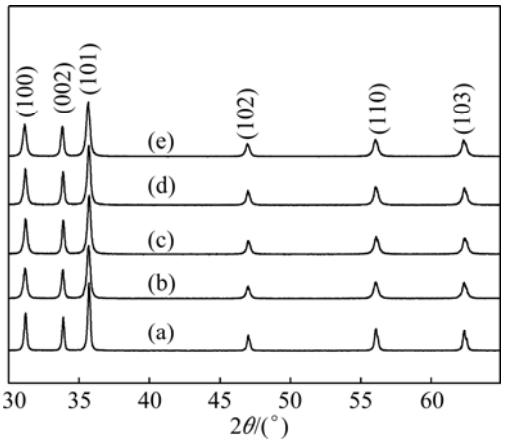

Fig. 1 XRD patterns of Ce-doped ZnO microspheres with different dopant contents: (a) 0; (b) 2%; (c) 4%; (d) 6%; (e) 10%

Figure 2 shows the surface morphologies of the pure and Ce-doped ZnO microspheres. The prepared products exhibit spherical shape with diameters ranging from 3 to 7 μm, which are assembled with radially aligned nanorods beyond several micrometers in length. As shown in Figs. 2(a_1) and (a_2), the nanorods with hexangular cross sections imply that the pure ZnO microspheres possess a high degree of crystallinity.

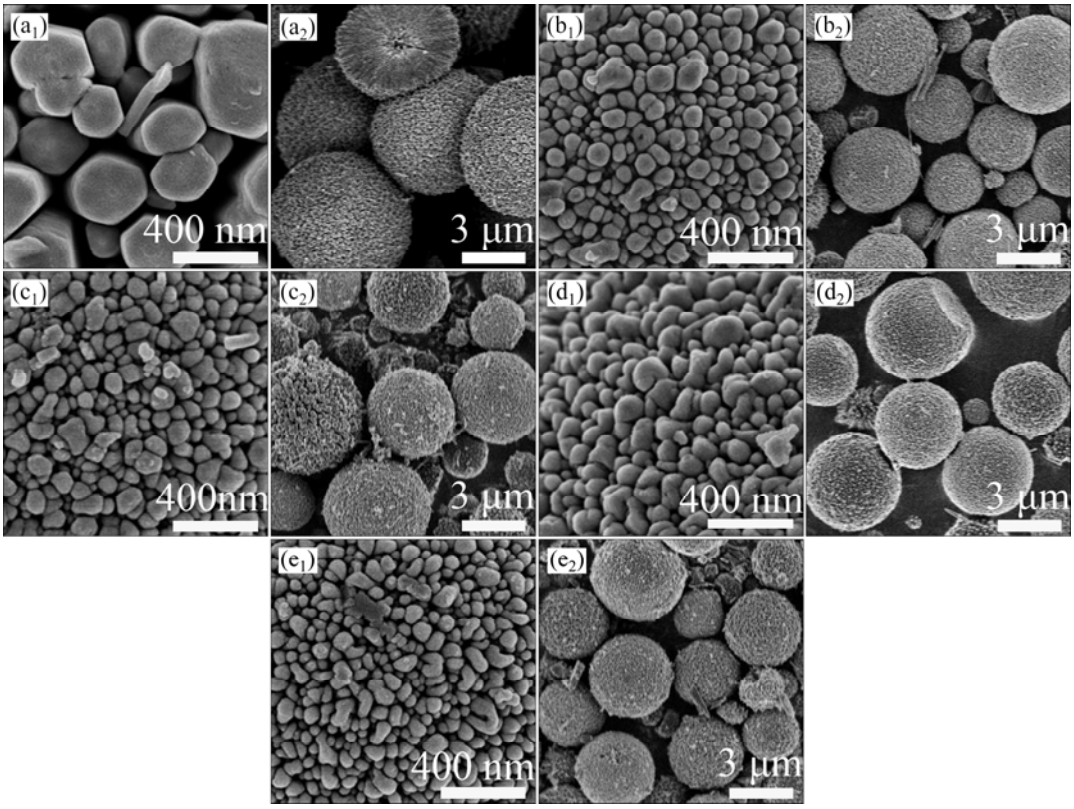

Fig. 2 Surface and overview SEM images of Ce-doped ZnO microspheres with different Ce contents: (a_1,a_2) 0; (b_1,b_2) 2%; (c_1,c_2) 4%; (d_1,d_2) 6%; (e_1,e_2) 10%

However, the diameter of nanorods greatly decreases to about 70 nm after introducing Ce into ZnO, as shown in Figs. 2(b_1), (c_1), (d_1) and (e_1). Moreover, the size of the microspheres also shows an obvious decrease after Ce doping, as shown in Figs. 2(b_2), (c_2), (d_2) and (e_2). It can be mainly assumed to the formation of Ce−O−Zn on the surface of Ce-doped microspheres, which restrained the growth of crystalline [22]. Obviously, the SEM images show a transition from loosely aligned nanorods of pure ZnO microspheres to tightly aligned nanorods after the Ce-doping. Furthermore, compared with the pure ZnO, the crystallinity for Ce-doped ZnO decreases according to the surface morphologies of nanorods in Figs. 2(b_1), (c_1), (d_1) and (e_1). Apparently, the lateral and polar growth of ZnO is remarkably restricted by doping 2% Ce into ZnO, and this trend does not develop with further increasing Ce-doping content. Figure 3 reveals that these microspheres have a hollow and radial structure that is composed of numerous nanorods, which have a perfect lath-shaped appearance (Fig. 3(c)) and a monocrystal structure (Fig. 3(d)).

Figure 4 shows the PL spectra of pure and Ce-doped samples excited by 325 nm at room temperature. All the samples exhibit UV and blue emission. The strong UV peak corresponds to the near-band-edge emission originating from the recombination of free excitons. The

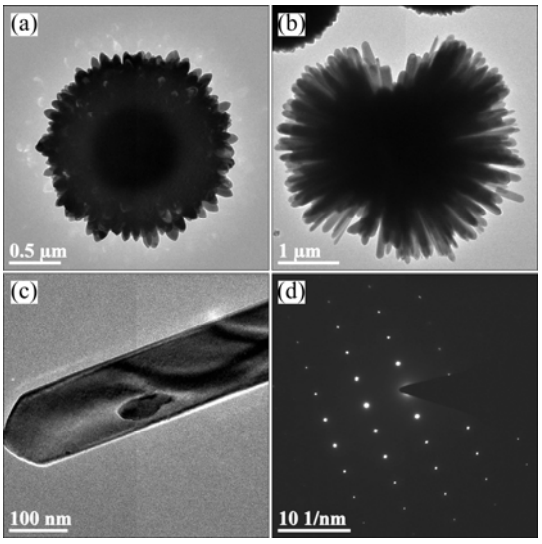

Fig. 3 TEM images of Ce-doped ZnO microspheres (a,b), single nano-rod (c) as component of microsphere and its electron diffraction pattern (d)

enhanced blue emission peaks at 452 nm and 470 nm are commonly attributed to the defects such as the transitions involved in zinc interstitials and oxygen vacancies in ZnO crystal [23]. Compared with the PL spectra of pure ZnO microspheres, the UV emission peaks for the Ce-doped ZnO exhibit obvious red shift while the

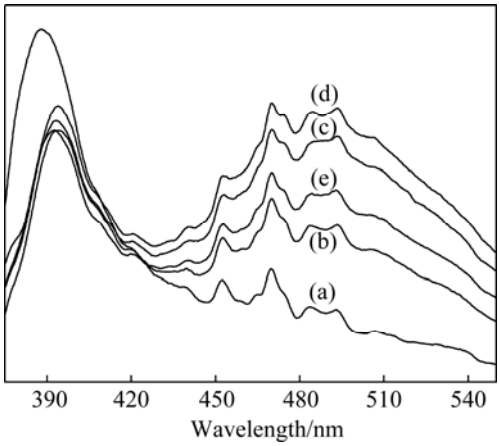

Fig. 4 PL spectra of pure ZnO (a) and Ce-doped ZnO microspheres with Ce contents of 2% (b), 4% (c), 6% (d) and 10% (e)

intensities are severely suppressed. This shift is due to the band gap narrowing caused by the downshift of the conduction band edge after merging with Ce-related impurity band formed below the conduction band [24]. Decreased UV emission peaks can be attributed to the increase of the defects and decrease of ZnO crystallite size [25]. Moreover, the intensities of visible emission are enhanced when the Ce content increases from 0 to 6%. It can be ascribed to the existence of Ce impurities in ZnO microspheres that might result in the formation of new defects such as Ce vacancies [26]. However, the intensities of visible emission decrease after further increasing Ce content to 10%.

Figure 5(a) exhibits the sensitivity of pure and Ce-doped ZnO microspheres to 50×10^{-6} ethanol at operating temperatures from 180 to 360 °C. Evidently, the sensitivities of all the samples to 50×10^{-6} ethanol increase with increasing operating temperature until the maximum value at 320 °C, and then begin to decrease with increasing temperature. Therefore, 320 °C was taken as the optimum operating temperature to proceed with the subsequent gas-sensing tests. It is well known that ZnO-based gas sensors are surface resistance control sensors, whose gas-sensing mechanism can be attributed to the changes of electrical conductivity resulting from the adsorption and desorption of oxygen molecules from the surface of nanocrystals. In air atmosphere, oxygen molecules are chemisorbed on the surface of ZnO microspheres and capture free electrons from the conduction band to form oxygen species (O^-, O^{2-}, and

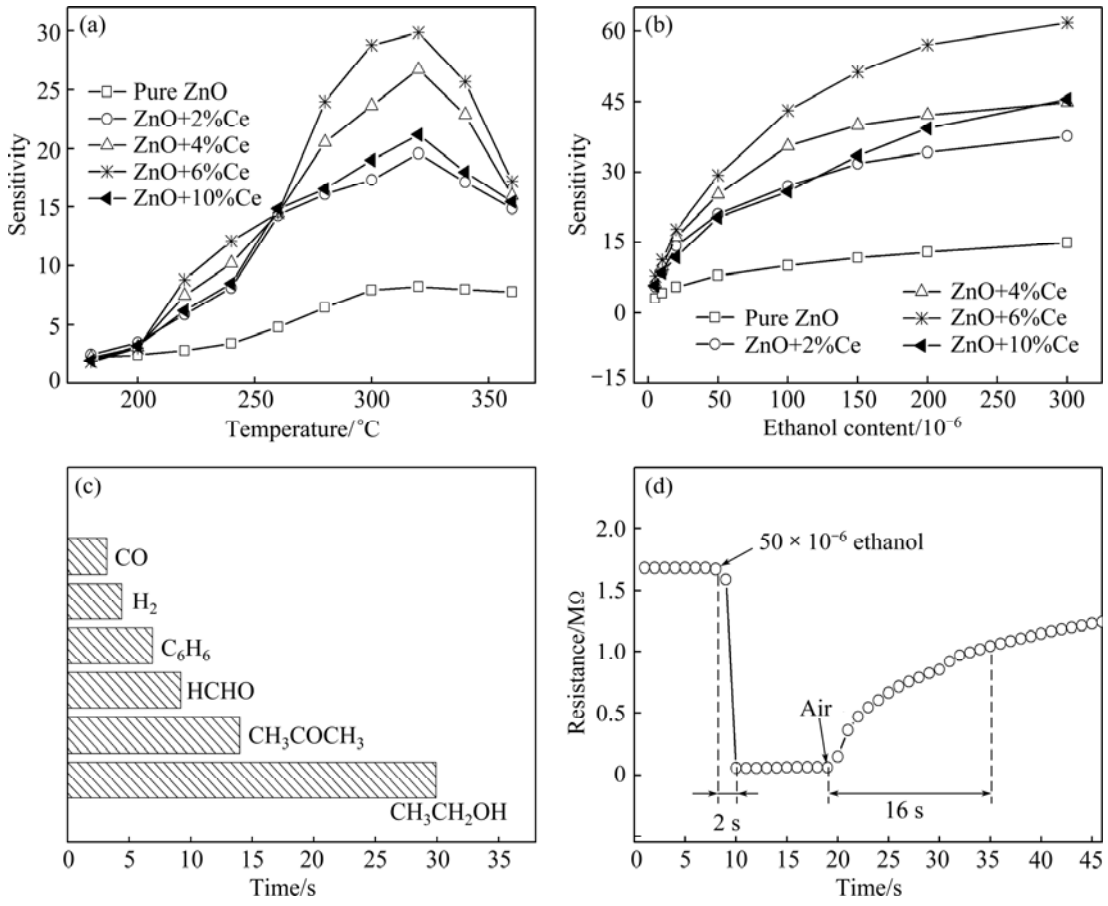

Fig. 5 Sensitivity of pure and Ce-doped ZnO microspheres to 50×10^{-6} ethanol at different operating temperatures (a), sensitivity of prepared samples versus ethanol content (b), sensitivity of Ce–ZnO microspheres doped with 6% Ce exposed to 50×10^{-6} gases (c), and response–recovery curve of Ce–ZnO microspheres doped with 6% Ce exposed to 50×10^{-6} ethanol at 320 °C (d)

O_2^-). Such process gives rise to surface depletion layers, which eventually decreases the electrical conductivity of ZnO microspheres. When ZnO microspheres are exposed to reducing gases, they can react with adsorbed oxygen species and release electrons to the conduction band, resulting in an increase in electrical conductivity. The surface reactions can be written as

$$O_2(gas) + e \rightleftharpoons O_2^-(ads) \quad (1)$$

$$O_2(gas) + 2e \rightleftharpoons 2O^-(ads) \quad (2)$$

$$O^-(ads) + e \rightleftharpoons O^{2-}(ads) \quad (3)$$

The content of chemically adsorbed oxygen species gradually increases with the increase of operating temperature, which results in the increasing variation of electrical conductivity. Therefore, the sensitivities are improved with the increasing temperature. However, the decrease in sensitivity above 320 °C is owing to the fact that the chemisorption is an exothermic reaction. If the temperature is further enhanced above 320 °C, the balance will move from adsorption to desorption, which leads to a decreased sensitivity [27]. Evidently, sensitivity of ZnO microspheres is improved with the addition of Ce and reaches a maximum value with 6% Ce. Further increase in Ce content results in a decreased sensitivity. For the pure ZnO, oxygen molecules are adsorbed on the surfaces and capture electrons from the conduction band, forming chemisorbed oxygen species O_2^-, O^- and O^{2-} as shown in Eqs. (1)−(3). When being exposed to ethanol, the ethanol molecules can react with adsorbed oxygen species in the following manner:

$$C_2H_5OH(gas)+6O^-(ads)\longrightarrow 2CO_2+3H_2O+6e \quad (4)$$

This process releases electrons to the conduction band, increasing electrical conductivity. Doping of ZnO with Ce will produce the oxygen vacancies that can provide more active adsorption sites. In addition, compared with pure ZnO microspheres, the Ce-doped ZnO microspheres will get more oxygen species on the surface owing to more oxygen vacancy related defects introduced by Ce doping, which can enhance the surface depletion thickness and the potential barrier height at the contact [28]. The oxygen molecules can interact strongly with oxygen vacancies on the surface of ZnO [29]. These suggest that the Ce doping can absorb more oxygen on the ZnO surface, which results in the enhanced sensitivity. Moreover, as for the morphology modification induced by Ce doping, it can play a vital role in the enhanced sensing performance. On one hand, the significant shrinkage in diameter of nanorods, which may cause an enhanced length/diameter ratio, will benefit the sensing properties [30]. On the other hand, the obvious decrease in the size of microspheres after Ce doping could also result in a higher sensitivity [31].

Figure 5(b) shows the sensitivity of pure and Ce-doped ZnO microspheres upon exposure to ethanol gas with a content of $(5-300)\times10^{-6}$ at 320 °C. The sensitivity tends to linearly increase when ethanol gas content ranges from 5×10^{-6} to 50×10^{-6}. The sensitivity increases drastically as the gas content increases to 150×10^{-6}. However, the sensitivity increases slowly when the content surpasses 150×10^{-6}, indicating that the sensors almost approach adsorption saturation due to the limited adsorption sites. It seems that Ce-doped ZnO sensors exhibit a higher sensitivity than pure ZnO sensor and they can detect ethanol down to 5×10^{-6}.

The sensitivity of 6%Ce-doped ZnO sensor to carbon monoxide (CO), hydrogen (H_2), benzene (C_6H_6), formaldehyde (HCHO), acetone (CH_3COCH_3) and ethanol (CH_3CH_2OH) with a content of 50×10^{-6} at 320 °C is revealed in Fig. 5(c). Obviously, the sensor was much less sensitive to acetone, formaldehyde and benzene and almost insensitive to hydrogen and carbon monoxide. Since ZnO can act as an acceptor for a long pair of electrons, organic vapors such as ethanol and acetone, which possess a long pair of electrons, have strong adsorption attraction on ZnO-based materials [32]. All these results show that the Ce-doped ZnO microspheres have good selectivity to ethanol.

In order to further investigate the practicability, the response−recovery characteristics of Ce−ZnO microspheres doped with 6% Ce exposure to 50×10^{-6} ethanol at 320 °C were also studied. The time for the sensor to reach 90% of the full resistance change is defined as the response time in the case of adsorption or the recovery time in the case of desorption. The sensor shows an excellent response of about 2 s and a moderate recovery of about 16 s (Fig. 5(d)), acceptable for applications of ethanol detection. This can be attributed to the enhanced active surface and accelerated gas diffusion induced by the porous structures of microspheres [33]. In this work, the enhanced gas sensing performance by Ce-doping could be explained as follows. Firstly, the resistance of the Ce-doped ZnO will decrease when Ce incorporates into ZnO to act as a donor; secondly, comparing with Zn^{2+}, Ce^{4+} in the higher valence state can increase the adsorption capacity of the surface of the Ce-doped ZnO, so that the resistance of the Ce-doped ZnO increases when exposing to air; in addition, the surface area of the Ce-doped ZnO increases when doping Ce into ZnO. Thus, the resistance change of the Ce-doped ZnO exposed to the atmosphere that from air to target gas is amplified. This also means that its gas sensing performance is naturally enhanced.

4 Conclusions

1) The SEM images show a transition from loose nanorods assembly of pure ZnO microspheres to tight nanorods assembly in Ce-doped microspheres after Ce-doping.

2) Effects of Ce-doping in the microspheres on optical properties show suppressed and red-shifted UV emission, and enhanced blue emission. Moreover, the intensities of visible emission are enhanced with the Ce content increasing from 0 to 6% and then decrease after doping with 10% Ce.

3) The gas-sensing results show that the sensitivity is dramatically enhanced after Ce-doping and the Ce-doped ZnO microspheres with Ce content of 6% exhibit the highest sensitivity to ethanol at 320 °C with quick response (2 s) and recovery time (16 s) to 50×10^{-6} ethanol gas.

References

[1] GREENE L E, YUHAS B D, LAW M, ZITOUN D, YANG P D. Solution-grown zinc oxide nanowires [J]. Inorganic Chemistry, 2006, 45: 7535−7543.

[2] LI Y, LIU C S, ZOU Y L. Growth mechanism and characterization of ZnO nano-tubes synthesized using the hydrothermal-etching method [J]. Chemical Papers, 2009, 63: 698−703.

[3] SAHAY P P, NATH R K. Al-doped ZnO thin films as methanol sensors [J]. Sensors and Actuators B—Chemical, 2008, 134: 654−659.

[4] ZHAO X, LOU F, LI M, LOU X, LI Z, ZHOU J. Sol−gel-based hydrothermal method for the synthesis of 3D flower-like ZnO microstructures composed of nanosheets for photocatalytic applications [J]. Ceramics International, 2014, 40: 5507−5514.

[5] ZHANG J, WANG S R, WANG Y, XU M J, XIA H J, ZHANG S M, HUANG W P, GUO X Z, WU S H. ZnO hollow spheres: Preparation, characterization, and gas sensing properties [J]. Sensors and Actuators B—Chemical, 2009, 139: 411−417.

[6] YAO Z N, SUN W J, LI W X, YANG H F, LI J J, GU C Z. Dual-gate field effect transistor based on ZnO nanowire with high-K gate dielectrics [J]. Microelectronic Engineering, 2012, 98: 343−346.

[7] FANG X, LI Y, ZHANG S, BAI L, YUAN N Y, DING J N. The dye adsorption optimization of ZnO nanorod-based dye-sensitized solar cells [J]. Solar Energy, 2014, 105: 14−19.

[8] BIAN J M, LIU W F, SUN J C, LIANG H W. Synthesis and defect-related emission of ZnO based light emitting device with homo- and hetero-structure [J]. Journal of Materials Processing Technology, 2007, 184: 451−454.

[9] LIU X, PAN K, LI W, HU D, LIU S, WANG Y. Optical and gas sensing properties of Al-doped ZnO transparent conducting films prepared by sol−gel method under different heat treatments [J]. Ceramics International, 2014, 40: 9931−9939.

[10] LI Yan, LI Guo-zhu, ZOU Yun-ling, WANG Qiong, ZHOU Qiu-jun, LIAN Xiao-xue. Preparation and sensing performance of petal-like RuO_2 modified ZnO nanosheets via a facile solvothermal and calcination method [J]. Transactions of Nonferrous Metals Society of China, 2014, 24(9): 2896−2903.

[11] ZHU S B, SHAN L M, TIAN X, ZHENG X Y, SUN D, LIU X B, WANG L, ZHOU Z W. Hydrothermal synthesis of oriented ZnO nanorod-nanosheets hierarchical architecture on zinc foil as flexible photoanodes for dye-sensitized solar cells [J]. Ceramics International, 2014, 40: 11663−11670.

[12] SONG P, WANG Q, YANG Z X. Acetone sensing characteristics of ZnO hollow spheres prepared by one-pot hydrothermal reaction [J]. Materials Letters, 2012, 86: 168−170.

[13] XU Y, YAO B, LI Y F, DING Z H, LI J C, WANG H Z, ZHANG Z Z, ZHANG L G, ZHAO H F, SHEN D Z. Chemical states of gold doped in ZnO films and its effect on electrical and optical properties [J]. Journal of Alloys and Compounds, 2014, 585: 479−484.

[14] PANG H L, ZHANG X H, ZHONG X X, LIU B, WEI X G, KUANG Y F, CHEN J H. Preparation of Ru-doped SnO_2-supported Pt catalysts and their electrocatalytic properties for methanol oxidation [J]. Journal of Colloid and Interface Science, 2008, 319: 193−198.

[15] KORAKE P V, KADAM A N, GARADKAR K M. Photocatalytic activity of Eu^{3+}-doped ZnO nanorods synthesized via microwave assisted technique [J]. Journal of Rare Earths, 2014, 32: 306−313.

[16] GUO J, ZHENG J, SONG X Z, SUN K. Synthesis and conductive properties of Ga-doped ZnO nanosheets by the hydrothermal method [J]. Materials Letters, 2013, 97: 34−36.

[17] YANG J H, GAO M, YANG L L, ZHANG Y J, LANG J H, WANG D D, WANG Y X, LIU H L, FAN H G. Low-temperature growth and optical properties of Ce-doped ZnO nanorods [J]. Applied Surface Science, 2008, 255: 2646−2650.

[18] WAN G X, MA S Y, LI X B, LI F M, BIAN H Q, ZHANG L P, LI W Q. Synthesis and acetone sensing properties of Ce-doped ZnO nanofibers [J]. Materials Letters, 2014, 114: 103−106.

[19] SIN J C, LAM S M, LEE K T, MOHAMED A R. Preparation of rare earth-doped ZnO hierarchical micro/nanospheres and their enhanced photocatalytic activity under visible light irradiation [J]. Ceramics International, 2014, 40: 5431−5440.

[20] HUSSAIN S, LIU T M, KASHIF M, LIN L Y, WU S F, GUO W W, ZENG W, HASHIM U. Effects of reaction time on the morphological, structural, and gas sensing properties of ZnO nanostructures [J]. Materials Science in Semiconductor Processing, 2014, 18: 52−58.

[21] MENG F, YIN J, DUAN Y Q, YUAN Z H, BIE L J. Co-precipitation synthesis and gas-sensing properties of ZnO hollow sphere with porous shell [J]. Sensors and Actuators B—Chemical, 2011, 156: 703−708.

[22] ANANDAN S, VINU A, MORI T, GOKULAKRISHNAN N, SRINIVASU P, MURUGESAN V, ARIGA K. Photocatalytic degradation of 2,4,6-trichlorophenol using lanthanum doped ZnO in aqueous suspension [J]. Catalysis Communications, 2007, 8: 1377−1382.

[23] ZENG H B, DUAN G T, LI Y, YANG S K, XU X X, CAI W P. Blue luminescence of ZnO nanoparticles based on non-equilibrium processes: defect origins and emission controls [J]. Advanced Functional Materials, 2010, 20: 561−572.

[24] MAJID A, ALI A. Red shift of near band edge emission in cerium implanted GaN [J]. Journal of Physics D—Applied Physics, 2009, 42: 045412.

[25] JEONG S H, KIM J K, LEE B T. Effects of growth conditions on the emission properties of ZnO films prepared on Si(100) by RF magnetron sputtering [J]. Journal of Physics D—Applied Physics, 2003, 36: 2017−2020.

[26] GONG H C, ZHONG J F, ZHOU S M, ZHANG B, LI Z H, DU Z L. Ce-induced single-crystalline hierarchical zinc oxide nanobrushes [J]. Superlattices and Microstructures, 2008, 44: 183−190.

[27] XU J Q, HA X H, LOU X D, XI G X, HAN H J, GAO Q H. Selective detection of HCHO gas using mixed oxides of $ZnO/ZnSnO_3$ [J]. Sensors and Actuators B—Chemical, 2007, 120: 694−699.

[28] CHANG C J, LIN C Y, CHEN J K, HSU M H. Ce-doped ZnO nanorods based low operation temperature NO_2 gas sensors [J].

Ceramics International, 2014, 40: 10867−10875.

[29] GURLO A. Interplay between O2 and SnO_2: Oxygen ionosorption and spectroscopic evidence for adsorbed oxygen [J]. Chem Phys Chem, 2006, 7: 2041−2052.

[30] GURAV K V, GANG M G, SHIN S W, PATIL U M, DESHMUKH P R, AGAWANE G L, SURYAWANSHI M P, PAWAR S M, PATIL P S, LOKHANDE C D, KIM J H. Gas sensing properties of hydrothermally grown ZnO nanorods with different aspect ratios [J]. Sensors and Actuators B—Chemical, 2014, 190: 439−445.

[31] SINGH R C, SINGH M P, SINGH O, CHANDI P S. Influence of synthesis and calcination temperatures on particle size and ethanol sensing behaviour of chemically synthesized SnO_2 nanostructures [J]. Sensors and Actuators B—Chemical, 2009, 143: 226−232.

[32] GONG H, WANG Y J, TEO S C, HUANG L. Interaction between thin-film tin oxide gas sensor and five organic vapors [J]. Sensors and Actuators B—Chemical, 1999, 54: 232−235.

[33] TIEMANN M. Porous metal oxides as gas sensors [J]. Chemistry—A European Journal, 2007, 13: 8376−8388.

铈掺杂氧化锌微球的形貌、光致发光和气敏性能

李 酽，刘金城，连晓雪，吕 谭，赵方贤

中国民航大学 理学院，天津 300300

摘 要：采用溶剂热法合成铈掺杂氧化锌微球。利用粉末 X 射线衍射仪、场发射扫描电子显微镜、透射电子显微镜、荧光光谱仪和气敏测试系统对样品的显微组织、形貌、发光和气敏性能进行表征。结果表明，铈掺杂氧化锌微球具有纤锌矿结构，由无数直径为 70 nm 的氧化锌棒组成。铈掺杂引起微球中棒状氧化锌由疏松排列向紧密排列结构演变。与纯氧化锌微球相比，铈掺杂氧化锌微球的紫外发光峰出现明显的红移，蓝色发光得到加强。在 320 ℃ 测试条件下，铈掺杂氧化锌微球对乙醇气体的灵敏度和选择性显著高于纯氧化锌微球。6% Ce 掺杂的氧化锌微球具有最高的灵敏度(约 30)，其对于 50×10^{-6} 的乙醇气体的响应和恢复时间分别为 2 s 和 16 s。

关键词：铈掺杂; 氧化锌；形貌；微球；气敏；光致发光

(Edited by Xiang-qun LI)